

Tangential oscillations of a circular disk in a viscous stratified fluid

ANTHONY M. J. DAVIS AND
STEFAN G. LLEWELLYN SMITH†

Department of Mechanical and Aerospace Engineering, Jacobs School of Engineering, UCSD,
9500 Gilman Drive, La Jolla, CA 92093-0411, USA

(Received 23 July 2009; revised 2 March 2010; accepted 4 March 2010;
first published online 21 May 2010)

A complete solution is obtained for the wave field generated by the time-harmonic edgewise oscillations of a horizontal circular disk in an incompressible stratified viscous fluid. The linearized equations of viscous internal waves and the no-slip condition on the rigid disk are used to derive sets of dual integral equations for the fluid velocity and vorticity. The dual integral equations are solved by analytic reduction to sets of linear algebraic equations. Asymptotic results confirm that this edgewise motion no longer excites waves in the small-viscosity limit. Broadside oscillations and the effect of density diffusion are also considered.

1. Introduction

The theory of internal waves has a long and rich history dating back at least to Rayleigh (1883). Internal waves play a critical role in atmospheric and ocean dynamics. For example, global and vertical ocean transport of heat, nutrients and dissolved gases is significantly influenced by mixing associated with the dissipation of internal tides, which are internal waves at tidal frequencies (Munk & Wunsch 1998; Garrett & Kunze 2007).

In parallel with theoretical and observational work, experimental studies have been crucial to improve our understanding of internal waves. Laboratory studies were pioneered by Görtler (1943), but those of Mowbray & Rarity (1967) led to much further work, most of which, at least until 2003, is reviewed by Voisin (2003). It is well known that the simplest possible experiment, namely oscillating a body in a stratified solution at a fixed frequency, produces the St Andrew's cross pattern (as seen on the cover of some printings of Lighthill 1978).

Laboratory experiments are naturally on a smaller scale than geophysical situations and viscosity is therefore expected to play a more important role. However, in one important respect, viscosity has not yet been treated fully consistently in theoretical work, even for the simplest linear generation problem. As discussed by Voisin (2003), previous studies have not applied the correct no-slip boundary condition but instead have carried out viscous calculations with free-slip boundary conditions (Hurley & Hood 1997; Hurley & Keady 1997) or applied the no-slip condition at a fictitious interface, with an iterative procedure to correct the latter approach (e.g. Vasil'ev & Chashechkin 2006, and a number of other papers by Chashechkin and collaborators).

† Email address for correspondence: sgls@ucsd.edu

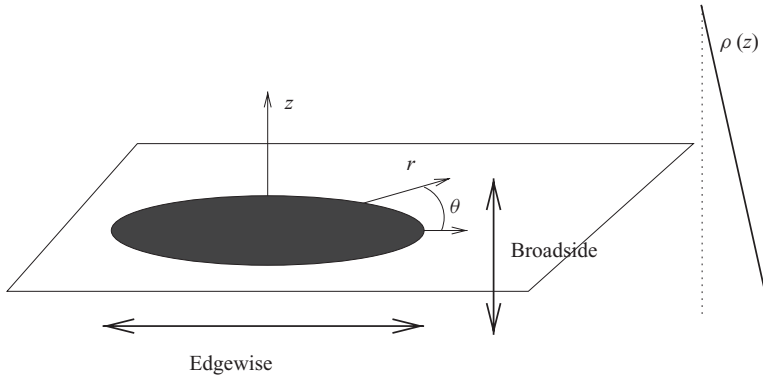


FIGURE 1. Cartoon of the geometry of this problem.

In this paper we provide the first consistent calculation of the linear internal waves generated by a moving object in a stratified fluid. Physical situations in which these results are expected to make a difference include laboratory experiments on internal wave generation by an oscillating disk using modern experimental techniques such as synthetic Schlieren. These techniques are now accurate enough for the inclusion of viscous effects in theoretical calculations to be necessary for quantitative agreement between prediction and experiment, as shown by experiments on a variety of body shapes (e.g. Sutherland & Linden 2002; Ermanyuk & Gavrilov 2008). We examine the time-harmonic wave field generated by a horizontal disk moving at constant frequency.

The focus of the analysis is the horizontal motion of the disk, i.e. tangential oscillations, in which case the viscosity is the sole generating mechanism: fluid is set in motion by the no-slip condition on the surface of the disk and without viscosity the bulk of the fluid remains at rest. In addition, vortex shedding, which cannot be considered here because of the restriction to small-amplitude motion, is unimportant. By contrast, vertical motion, i.e. broadwise oscillations, generates a wave field that is more likely to exhibit vortex shedding at higher Reynolds numbers. Figure 1 shows the geometry under consideration. We do not consider twisting of the disk, just translation parallel and normal to the disk.

The governing parameters are the radius of the disk (a), the frequency of oscillation ω , the buoyancy frequency N and the fluid's kinematic viscosity ν . The Boussinesq approximation is taken and N is assumed to be constant in the vertical. The velocity of the disk v_0 does not enter the solution except as a scaling factor because of the linearization: we are assuming that the Keulegan–Carpenter number av_0/ν is small. Then the remaining parameters can be grouped into the two dimensionless quantities: N/ω and $(\nu/\omega)^{1/2}/a$.

The analysis in this paper covers the entire parameter space spanned by these two quantities. The limit $N=0$ recovers oscillatory Stokes flow, while small $(\nu/\omega)^{1/2}/a$ corresponds to inviscid internal waves, with the general case being that of viscous internal waves.

In §2 we obtain the solution to the problem in terms of two unknown functions that satisfy coupled dual integral equations. This derivation is related to that in Davis & Nagem (2004). We transform these equations into an infinite set of linear equations in §3. Results are presented in §4, starting with an asymptotic approximation for the far-field radiated pressure and the behaviour of the force on the disk for small and

large Stokes numbers. This is followed by numerical results over a range of parameter values, showing the effects of viscosity on the force on the disk and on the radiated wave field. Results for vertical motion of the disk are presented in §5, while the effect of density diffusion is examined in §6. Finally we summarize in §7.

2. Theory

The standard Boussinesq equations for linearized flow in a homogeneous, stratified, non-rotating, viscous fluid are the continuity equation

$$\nabla \cdot \mathbf{v} = 0, \quad (2.1)$$

the momentum equation

$$\frac{\partial \mathbf{v}}{\partial t} = -\frac{1}{\rho_0} \nabla p + \nu \nabla^2 \mathbf{v} - \frac{\rho}{\rho_0} g \mathbf{e}_z, \quad (2.2)$$

and the buoyancy equation

$$\frac{\partial \rho}{\partial t} = \rho_0 \frac{N^2}{g} \mathbf{v} \cdot \mathbf{e}_z. \quad (2.3)$$

Here \mathbf{v} is the fluid velocity vector, $N = [-(g/\rho_0)(d\rho_B/dz)]^{1/2}$ is the buoyancy frequency where ρ_B is the background hydrostatic fluid density and ρ_0 is a reference density, ρ is the density perturbation, p is the fluid pressure and ν is the kinematic viscosity. With N assumed to be constant, it may be deduced from (2.1)–(2.3) that the vorticity $\boldsymbol{\Omega}$ satisfies

$$\frac{\partial}{\partial t} \left(\frac{\partial}{\partial t} - \nu \nabla^2 \right) \boldsymbol{\Omega} + N^2 \nabla \times [(\mathbf{v} \cdot \mathbf{e}_z) \mathbf{e}_z] = 0, \quad (2.4)$$

while p is determined from the flow field by

$$\frac{\partial}{\partial t} \nabla^2 p + N^2 \rho_0 \frac{\partial}{\partial z} (\mathbf{v} \cdot \mathbf{e}_z) = 0. \quad (2.5)$$

These are the governing equations for viscous stratified flow.

A horizontally oriented rigid disk is at $z=0$, $0 \leq r < a$ and, due to the fluid viscosity, generates a three-dimensional disturbance by oscillating in its own plane with velocity amplitude v_0 and period $2\pi/\omega$. The dimensionless quantity $a^2\omega/\nu$, sometimes called the Stokes number, need not be large and may well be $O(1)$ in laboratory experiments. After suppressing the time factor $e^{-i\omega t}$, the no-slip condition $\mathbf{v} = v_0 \mathbf{e}_x$ at the disk implies that the cylindrical velocity components $v_0(V_r \cos \theta, V_\theta \sin \theta, V_z \cos \theta)$ satisfy

$$V_r = 1, \quad V_\theta = -1, \quad V_z = 0 \quad \text{at } z = 0, \quad 0 \leq r < a. \quad (2.6)$$

Also, the stress discontinuities are confined to the disk. The calculation of the velocity field, which evidently is such that $V_z=0$ in the plane $z=0$ of the vibrating disk, is simplified by its confinement to the first Fourier mode but complicated by the imposed stratification. We are able to eschew the use of scalar potentials by working from the vorticity field in an arguably more direct construction of the radiated wave field.

Equation (2.4) implies that the vorticity components $v_0(\Omega_r \sin \theta, \Omega_\theta \cos \theta, \Omega_z \sin \theta)$ are governed by

$$\left(\frac{\partial^2}{\partial r^2} + \frac{1}{r} \frac{\partial}{\partial r} + \frac{\partial^2}{\partial z^2} + \frac{i\omega}{v}\right) \begin{bmatrix} \Omega_z \\ \Omega_r + \Omega_\theta \\ \Omega_r - \Omega_\theta \end{bmatrix} = \frac{1}{r^2} \begin{bmatrix} \Omega_z \\ 0 \\ 4(\Omega_r - \Omega_\theta) \end{bmatrix} + \frac{N^2}{i\omega v} \begin{bmatrix} 0 \\ \frac{V_z}{r} + \frac{\partial V_z}{\partial r} \\ \frac{V_z}{r} - \frac{\partial V_z}{\partial r} \end{bmatrix}. \tag{2.7}$$

Suitable solutions, with Ω_z an even function of z , are the Hankel transforms given by

$$\Omega_z = \int_0^\infty \frac{kB(k)}{(k^2 - i\omega/v)^{1/2}} e^{-(k^2 - i\omega/v)^{1/2}|z|} J_1(kr) dk, \tag{2.8}$$

and, since $\nabla \cdot \boldsymbol{\Omega} = 0$ implies that

$$\frac{\partial}{\partial r}(\Omega_r + \Omega_\theta) + \frac{1}{r^2} \frac{\partial}{\partial r}[r^2(\Omega_r - \Omega_\theta)] + 2 \frac{\partial \Omega_z}{\partial z} = 0, \tag{2.9}$$

$$\Omega_r + \Omega_\theta = \text{sgn}(z) \int_0^\infty [F(k, z) - B(k)e^{-(k^2 - i\omega/v)^{1/2}|z|}] J_0(kr) dk, \tag{2.10}$$

$$\Omega_r - \Omega_\theta = \text{sgn}(z) \int_0^\infty [F(k, z) + B(k)e^{-(k^2 - i\omega/v)^{1/2}|z|}] J_2(kr) dk, \tag{2.11}$$

where $F(k, z)$ is a function to be determined. Substitution of (2.10) and (2.11) into (2.7) gives two equations for V_z which yield

$$V_z = \frac{i\omega v}{N^2} \text{sgn}(z) \int_0^\infty \left[\frac{d^2 F}{dz^2} - \left(k^2 - \frac{i\omega}{v}\right) F \right] \frac{J_1(kr)}{k} dk. \tag{2.12}$$

Then, because the horizontal vorticity components are defined in terms of the velocity components by

$$\Omega_r + \Omega_\theta = -\frac{1}{r} \frac{\partial}{\partial r}(rV_z) + \frac{\partial}{\partial z}(V_r - V_\theta), \tag{2.13}$$

$$\Omega_r - \Omega_\theta = r \frac{\partial}{\partial r} \left(\frac{1}{r} V_z \right) - \frac{\partial}{\partial z}(V_r + V_\theta), \tag{2.14}$$

the z -derivative of

$$\frac{\partial}{\partial r}(V_r - V_\theta) + \frac{1}{r^2} \frac{\partial}{\partial r}[r^2(V_r + V_\theta)] + 2 \frac{\partial V_z}{\partial z} = 0, \tag{2.15}$$

obtained from (2.1), facilitates deduction of the relation

$$\frac{\partial}{\partial r}(\Omega_r + \Omega_\theta) - \frac{1}{r^2} \frac{\partial}{\partial r}[r^2(\Omega_r - \Omega_\theta)] + 2 \left(\frac{\partial^2 V_z}{\partial r^2} + \frac{1}{r} \frac{\partial V_z}{\partial r} + \frac{\partial^2 V_z}{\partial z^2} - \frac{V_z}{r^2} \right) = 0. \tag{2.16}$$

When the vorticity components in (2.10) and (2.11) and V_z in (2.12) are substituted, it is found that F is governed by

$$\left(\frac{d^2}{dz^2} - k^2 \right) \left(\frac{d^2}{dz^2} - k^2 + \frac{i\omega}{v} \right) F + \frac{iN^2 k^2}{\omega v} F = 0. \tag{2.17}$$

Hence, F is a linear combination of $e^{-\lambda_1|z|}$, $e^{-\lambda_2|z|}$, where

$$\text{Re}(\lambda_1) > 0, \quad \text{Re}(\lambda_2) > 0, \quad \left. \begin{matrix} \lambda_1^2 \\ \lambda_2^2 \end{matrix} \right\} = k^2 - \frac{i\omega}{2v} \pm i \sqrt{\frac{\omega^2}{4v^2} + \frac{iN^2 k^2}{\omega v}}. \tag{2.18}$$

Because V_z vanishes in the plane $z=0$, it follows that (2.12) may be written as

$$V_z = -\operatorname{sgn}(z) \int_0^\infty \frac{iC(k)}{\sqrt{\frac{\omega^2}{4\nu^2} + \frac{iN^2k^2}{\omega\nu}}} [e^{-\lambda_1|z|} - e^{-\lambda_2|z|}] kJ_1(kr) dk, \quad (2.19)$$

whence, by using (2.18),

$$\begin{aligned} F &= -\frac{C(k)}{\sqrt{\frac{\omega^2}{4\nu^2} + \frac{iN^2k^2}{\omega\nu}}} \left[\frac{e^{-\lambda_1|z|}}{\lambda_1^2 - k^2 + \frac{i\omega}{\nu}} - \frac{e^{-\lambda_2|z|}}{\lambda_2^2 - k^2 + \frac{i\omega}{\nu}} \right] \frac{N^2k^2}{\omega\nu} \\ &= -\frac{iC(k)}{\sqrt{\frac{\omega^2}{4\nu^2} + \frac{iN^2k^2}{\omega\nu}}} [(\lambda_1^2 - k^2)e^{-\lambda_1|z|} - (\lambda_2^2 - k^2)e^{-\lambda_2|z|}]. \end{aligned} \quad (2.20)$$

After substitution of (2.20) into (2.10) and (2.11), (2.13), (2.14) and (2.19) now yield

$$V_r - V_\theta = \int_0^\infty \left\{ \frac{iC(k)}{\sqrt{\frac{\omega^2}{4\nu^2} + \frac{iN^2k^2}{\omega\nu}}} [\lambda_1 e^{-\lambda_1|z|} - \lambda_2 e^{-\lambda_2|z|}] + \frac{B(k)}{(k^2 - i\omega/\nu)^{1/2}} e^{-(k^2 - i\omega/\nu)^{1/2}|z|} \right\} J_0(kr) dk, \quad (2.21)$$

$$V_r + V_\theta = \int_0^\infty \left\{ -\frac{iC(k)}{\sqrt{\frac{\omega^2}{4\nu^2} + \frac{iN^2k^2}{\omega\nu}}} [\lambda_1 e^{-\lambda_1|z|} - \lambda_2 e^{-\lambda_2|z|}] + \frac{B(k)}{(k^2 - i\omega/\nu)^{1/2}} e^{-(k^2 - i\omega/\nu)^{1/2}|z|} \right\} J_2(kr) dk. \quad (2.22)$$

Equations (2.21) and (2.22) show that the Helmholtz decomposition,

$$V_r = \frac{\partial\Phi}{\partial r} + \frac{\Psi}{r}, \quad V_\theta = -\frac{\partial\Psi}{\partial r} - \frac{\Phi}{r}, \quad (2.23)$$

of the horizontal velocity field is such that

$$\Phi = \int_0^\infty \frac{iC(k)}{\sqrt{\frac{\omega^2}{4\nu^2} + \frac{iN^2k^2}{\omega\nu}}} [\lambda_1 e^{-\lambda_1|z|} - \lambda_2 e^{-\lambda_2|z|}] \frac{J_1(kr)}{k} dk, \quad (2.24)$$

$$\Psi = \int_0^\infty \frac{B(k)}{(k^2 - i\omega/\nu)^{1/2}} e^{-(k^2 - i\omega/\nu)^{1/2}|z|} \frac{J_1(kr)}{k} dk. \quad (2.25)$$

It is possible to work from the outset using potentials related to wave-vortex decompositions of stratified flow (Kistovich & Chashechkin 2001; Voisin 2003), but the functions $C(k)$ and $B(k)$ provide the simplest framework here.

The unknown functions $C(k)$, $B(k)$ are now determined by imposing the prescribed disk velocity and requiring no net stress discontinuities at $z=0$, $r>a$. It is readily

seen from (2.18), (2.21) and (2.22) that (2.6) is satisfied provided

$$\int_0^\infty \left[-\frac{2C(k)}{\lambda_1 + \lambda_2} + \frac{B(k)}{(k^2 - i\omega/\nu)^{1/2}} \right] J_0(kr) dk = 2, \quad (r < a), \tag{2.26}$$

$$\int_0^\infty \left[\frac{2C(k)}{\lambda_1 + \lambda_2} + \frac{B(k)}{(k^2 - i\omega/\nu)^{1/2}} \right] J_2(kr) dk = 0, \quad (r < a). \tag{2.27}$$

After deducing from (2.5), (2.19) that the pressure is given by

$$p = \frac{N^2}{\omega} \rho_0 v_0 \cos \theta \int_0^\infty \frac{C(k)}{\sqrt{\frac{\omega^2}{4\nu^2} + \frac{iN^2 k^2}{\omega\nu}}} \left[\frac{\lambda_1 e^{-\lambda_1 |z|}}{\lambda_1^2 - k^2} - \frac{\lambda_2 e^{-\lambda_2 |z|}}{\lambda_2^2 - k^2} \right] k J_1(kr) dk, \tag{2.28}$$

it is evident that the in-plane oscillations cannot generate a normal stress disparity at the disk, and equations valid for $r > a$ are obtained by considering the tangential stresses at the plane $z = 0$. Their discontinuities are, according to the solutions (2.21) and (2.22), confined to the disk provided

$$\int_0^\infty [-2C(k) + B(k)] J_0(kr) dk = 0, \quad (r > a), \tag{2.29}$$

$$\int_0^\infty [2C(k) + B(k)] J_2(kr) dk = 0, \quad (r > a). \tag{2.30}$$

The pairs (2.26)–(2.27) and (2.29)–(2.30) are identified as dual integral equations for $C(k)$ and $B(k)$. As expected, they have the same structure as the $n = 1$ cases of (27) and (30) in Davis & Nagem (2004).

3. The radiated field: solution by Tranter’s method

As shown by Tanzosh & Stone (1995), the coupled pairs above can be directly converted into linear algebraic equations. Tranter’s method (Tranter 1966) starts with the key observation that

$$A(u) = u^\alpha \sum_{m=0}^\infty a_m J_{\nu-\alpha+2m+1}(u) \tag{3.1}$$

satisfies

$$\int_0^\infty A(u) J_\nu(xu) du = 0, \quad (x > 1) \tag{3.2}$$

for $|\alpha| < 1$ and arbitrary a_m . Explicit expressions for the coefficients are available when the integrand for the interval $x < 1$ has only the additional factor $u^{-2\alpha}$. Otherwise, the choice of α is determined by the behaviour of the additional factor as $u \rightarrow \infty$. So, because the velocities introduce a factor that is $O(k^{-1})$ as $k \rightarrow \infty$, $\alpha = 1/2$ here. Thus, equations (2.29) and (2.30) are satisfied by writing

$$\mp 2C(k) + B(k) = (ka)^{1/2} \sum_{m=0}^\infty (\mp 2c_m + b_m) J_{2m+1/2}(ka), \quad (2c_0 + b_0 = 0); \tag{3.3}$$

we shall find the coefficients c_m and b_m from the remaining integral equations. After substituting (3.3) and writing $u = ka$, $r = a\xi$, $a[\lambda_1(k) + \lambda_2(k)] = 2\Lambda(u)$, (2.26) and (2.27)

become

$$\sum_{m=0}^{\infty} \int_0^{\infty} \left[\mp \frac{c_m}{\Lambda(u)} + \frac{b_m}{(u^2 - ia^2\omega/\nu)^{1/2}} \right] u^{1/2} J_{2m+1/2}(u) J_{1\mp 1}(u\xi) du = 1 \pm 1, \quad (\xi < 1). \tag{3.4}$$

Tranter’s method, described in Sneddon (1966, § 4.6), now transforms these functional identities into linear algebraic equations by using

$$\frac{2^{1/2} \Gamma(\nu + l + 1)}{\Gamma(\nu + 1)\Gamma(l + 1/2)} \int_0^1 \frac{\xi^{\nu+1}}{(1 - \xi^2)^{1/2}} \mathcal{F}_l(\nu + 1/2, \nu + 1; \xi^2) J_{\nu}(u\xi) d\xi = u^{-1/2} J_{2l+\nu+1/2}(u), \tag{3.5}$$

with $\nu = 0, 2$ respectively and \mathcal{F}_l a Jacobi polynomial, to obtain (for $l \geq 0$)

$$\sum_{m=0}^{\infty} \int_0^{\infty} \left[-\frac{c_m}{\Lambda(u)} + \frac{b_m}{(u^2 - ia^2\omega/\nu)^{1/2}} \right] J_{2m+1/2}(u) J_{2l+1/2}(u) du = 2\delta_{l0} \sqrt{\frac{2}{\pi}}, \tag{3.6}$$

$$\sum_{m=0}^{\infty} \int_0^{\infty} \left[\frac{c_m}{\Lambda(u)} + \frac{b_m}{(u^2 - ia^2\omega/\nu)^{1/2}} \right] J_{2m+1/2}(u) J_{2l+5/2}(u) du = 0. \tag{3.7}$$

Non-dimensionalization has been eschewed to this point because the governing equations have length scale determined by viscous oscillations while the disk radius is the length scale of the mixed boundary conditions. With the application of Tranter’s method now complete, the role of the Stokes number, $S^2 = a^2\omega/\nu$, is elucidated by writing $u = Sv$, that is $\nu = k\sqrt{\nu/\omega}$, in (2.18) to obtain

$$\text{Re}(\lambda_1) > 0, \quad \text{Re}(\lambda_2) > 0, \quad \left. \begin{matrix} (a\lambda_1)^2 \\ (a\lambda_2)^2 \end{matrix} \right\} = S^2 \left[v^2 - \frac{i}{2} \pm i\sqrt{\frac{1}{4} + \frac{iN^2v^2}{\omega^2}} \right], \tag{3.8}$$

and in the linear system (3.6) and (3.7) to obtain (again for $l \geq 0$)

$$\sum_{m=0}^{\infty} \int_0^{\infty} \left[-\frac{Sc_m}{\Lambda(Sv)} + \frac{b_m}{(v^2 - i)^{1/2}} \right] J_{2m+1/2}(Sv) J_{2l+1/2}(Sv) dv = 2\delta_{l0} \sqrt{\frac{2}{\pi}}, \tag{3.9}$$

$$\sum_{m=0}^{\infty} \int_0^{\infty} \left[\frac{Sc_m}{\Lambda(Sv)} + \frac{b_m}{(v^2 - i)^{1/2}} \right] J_{2m+1/2}(Sv) J_{2l+5/2}(Sv) dv = 0. \tag{3.10}$$

The system is completed by $2c_0 + b_0 = 0$ and (3.8) yields $2D(v) = [2v^2 - i + 2v\sqrt{v^2 + i(N^2/\omega^2 - 1)}]^{1/2}$ where $D(v) = S^{-1}\Lambda(Sv)$, which shows that S appears in only the Bessel function arguments.

The tangential stress yields a drag force given by

$$\mathbf{F} = -\pi e^{-i\omega t} \mathbf{e}_x \rho_0 \nu v_0 \int_0^a \left[\frac{\partial}{\partial z} (V_r - V_{\theta}) \right]_{z=0-}^{0+} r dr = 2\sqrt{2\pi}(-2c_0 + b_0) e^{-i\omega t} \mathbf{e}_x \rho_0 \nu v_0 a, \tag{3.11}$$

after substitution of (2.22). In what follows we use the non-dimensionalized x -component of \mathbf{F} given by $F_x = 2\sqrt{2\pi}(-2c_0 + b_0)$.

4. Results

4.1. Far-field pressure

The radiated pressure, given by (2.28), can be estimated in the far field by using the small- k approximations,

$$\lambda_1^2 \sim k^2 \left(1 - \frac{N^2}{\omega^2}\right), \quad \lambda_2^2 \sim -\frac{i\omega}{\nu}, \quad C(k) \sim c_0 \sqrt{\frac{2}{\pi}} \sin(ka), \tag{4.1}$$

deduced from (2.18) and (3.3), to obtain, for $\omega > N$, $r^2 + z^2 \gg \nu/\omega$ and $r^2 + z^2 \gg a^2$,

$$p \sim -2c_0 \sqrt{\frac{2}{\pi}} \rho_0 \nu v_0 \cos \theta \int_0^\infty \left(1 - \frac{N^2}{\omega^2}\right)^{1/2} e^{-k|z|(1-N^2/\omega^2)^{1/2}} J_1(kr) \sin ka \, dk \tag{4.2}$$

and hence

$$p \sim -2c_0 \sqrt{\frac{2}{\pi}} \rho_0 \nu a v_0 \cos \theta \frac{\left(1 - \frac{N^2}{\omega^2}\right)^{1/2} r}{\left[r^2 + \left(1 - \frac{N^2}{\omega^2}\right) z^2\right]^{3/2}}. \tag{4.3}$$

If $\omega < N$, the integrand lacks exponential decay and more care is required. Note that λ_1 must lie in the first quadrant because

$$\lambda_1^2 = k^2 + \frac{i\omega}{2\nu}(\xi - 1 + i\eta), \quad (0 < \eta < \xi), \tag{4.4}$$

where $\xi^2 - \eta^2 = 1$ and $\xi\eta = 2N^2k^2\nu/\omega^3$. Thus, $\lambda_1 \sim ik\sqrt{N^2/\omega^2 - 1}$ in (4.1) and so

$$\begin{aligned} p &\sim 2c_0 \sqrt{\frac{2}{\pi}} \rho_0 \nu v_0 \frac{\partial}{\partial x} \int_0^\infty i \left(\frac{N^2}{\omega^2} - 1\right)^{1/2} e^{-ik|z|(N^2/\omega^2 - 1)^{1/2}} J_0(kr) \frac{\sin ka}{k} \, dk \\ &\sim 2c_0 \sqrt{\frac{2}{\pi}} \rho_0 \nu a v_0 \frac{\partial}{\partial x} \left(\frac{N^2}{\omega^2} - 1\right)^{1/2} \begin{cases} \left[\left(\frac{N^2}{\omega^2} - 1\right) z^2 - r^2\right]^{-1/2} & [N|z| > \omega(r^2 + z^2)^{1/2}] \\ i \left[r^2 - \left(\frac{N^2}{\omega^2} - 1\right) z^2\right]^{-1/2} & [N|z| < \omega(r^2 + z^2)^{1/2}], \end{cases} \end{aligned} \tag{4.5}$$

except near the St Andrew’s cone. The apparent singular behaviour in (4.5) is mitigated, as in Voisin (2003), by using the more accurate small- k approximation,

$$\lambda_1 \sim k \left(\frac{N^2}{\omega^2} - 1\right)^{1/2} \left[i + \frac{N^4 k^2 \nu}{2\omega^3(N^2 - \omega^2)} \right]. \tag{4.6}$$

On setting $\omega = N \cos \phi_0$, (4.5) is then replaced by

$$\begin{aligned} p &\sim 2c_0 \sqrt{\frac{2}{\pi}} \rho_0 \nu a v_0 \frac{\partial}{\partial x} \int_0^\infty i \tan \phi_0 e^{-ik|z| \tan \phi_0} J_0(kr) \exp \left[-\frac{\nu|z|k^3}{2\omega \cos^3 \phi_0 \sin \phi_0} \right] \, dk \\ &\sim 2c_0 \sqrt{\frac{2}{\pi}} \rho_0 \nu a v_0 \frac{\partial}{\partial x} i \sin \phi_0 \left(\frac{2\omega \sin \phi_0}{3\nu|z|}\right)^{1/3} \\ &\times \int_0^\pi \text{Hi} \left[i \left(\frac{2\omega \sin \phi_0}{3\nu|z|}\right)^{1/3} (r \cos \alpha \cos \phi_0 - |z| \sin \phi_0) \right] \, d\alpha, \end{aligned} \tag{4.7}$$

in which $(r \cos \alpha \cos \phi_0 - |z| \sin \phi_0)$ is identified as the projection of the position vector $(r \cos \alpha, r \sin \alpha, |z|)$ on the typical normal, $(\cos \phi_0, 0, -\sin \phi_0)$, to the St Andrew’s cone,

and Hi denotes the Airy function defined (Abramowitz & Stegun 1965, (10.4.4)) by

$$\text{Hi}(Z) = \frac{1}{\pi} \int_0^\infty e^{uZ-u^3/3} du. \tag{4.8}$$

As expected, this far-field pressure estimate is also obtained when the disturbance is generated by the drag force in (3.11) applied at the origin. The asymptotic result (4.7) can be viewed as the generalization of the Thomas & Stevenson (1972) similarity solution to a three-dimensional situation forced by an oscillating object.

When $\omega = N$, the above results do not apply and a viscous calculation is needed to obtain the asymptotic behaviour, as in Gordon & Stevenson (1972). We find $\lambda_1^2 \sim k^4(iv/\omega)$. Thus,

$$p \sim c_0 \sqrt{\frac{2}{\pi}} \rho_0 v a v_0 |z|^{-1} \frac{\partial}{\partial x} \exp \left[-e^{-i\pi/4} \sqrt{\frac{\omega}{v}} \frac{r^2}{4|z|} \right]. \tag{4.9}$$

Hence, the pressure is exponentially small except in a parabolic region near the z -axis. It vanishes on the z -axis to this order.

4.2. *Asymptotic results for the force on the disk*

If S^2 is not large, the evaluation of the semi-infinite integrals is facilitated by noting that $2\Lambda(u) = a[\lambda_1(k) + \lambda_2(k)] \sim 2ka = 2u$ as $u \rightarrow \infty$ and making use of the identity

$$\int_0^\infty \frac{J_{2m+1/2}(Sv)J_{2l+1/2}(Sv)}{v} dv = \frac{\delta_{ml}}{4m+1}. \tag{4.10}$$

This has the advantage of giving the dominant contribution to the diagonal terms in (3.9) and (3.10) in a closed form. The result is

$$\begin{aligned} & \frac{-c_l + b_l}{4l+1} - \sum_{m=0}^\infty c_m \int_0^\infty \left[\frac{S}{\Lambda(Sv)} - \frac{1}{v} \right] J_{2m+1/2}(Sv)J_{2l+1/2}(Sv) dv \\ & + \sum_{m=0}^\infty b_m \int_0^\infty \left[\frac{1}{(v^2-i)^{1/2}} - \frac{1}{v} \right] J_{2m+1/2}(Sv)J_{2l+1/2}(Sv) dv = 2\delta_{l0} \sqrt{\frac{2}{\pi}}, \end{aligned} \tag{4.11}$$

$$\begin{aligned} & \frac{c_{l+1} + b_{l+1}}{4l+5} + \sum_{m=0}^\infty c_m \int_0^\infty \left[\frac{S}{\Lambda(Sv)} - \frac{1}{v} \right] J_{2m+1/2}(Sv)J_{2l+5/2}(Sv) dv \\ & + \sum_{m=0}^\infty b_m \int_0^\infty \left[\frac{1}{(v^2-i)^{1/2}} - \frac{1}{v} \right] J_{2m+1/2}(Sv)J_{2l+5/2}(Sv) dv = 0, \end{aligned} \tag{4.12}$$

with the system completed by $2c_0 + b_0 = 0$.

The $O(1)$ solution, $b_0 - c_0 = 2\sqrt{2/\pi}$, substituted into (3.11), yields the known zero-frequency limit value, $\mathbf{F} = (32/3)e_x \rho_0 v v_0 a$, for an edgewise translating disk in creeping flow. The $O(S)$ correction term arises solely from the $m=0=l$ terms. The integrals multiplying b_0 and c_0 respectively in (4.12) give

$$\int_0^\infty \left[\frac{1}{(v^2-i)^{1/2}} - \frac{1}{v} \right] J_{1/2}(Sv)J_{1/2}(Sv) dv \sim \frac{2}{\pi} e^{3i\pi/4} S = \beta S, \tag{4.13}$$

as in Davis (1993), and

$$\int_0^\infty \left[\frac{S}{\Lambda(Sv)} - \frac{1}{v} \right] J_{1/2}(Sv)J_{1/2}(Sv) dv \sim \frac{2S}{\pi} \int_0^\infty \left[\frac{Sv}{\Lambda(Sv)} - 1 \right] dv = \gamma S, \tag{4.14}$$

with $\gamma(\omega/N)$ available in a closed form (the expression is so complicated however that it was not used and instead γ was computed numerically). The infinite set of matrix equations can then be truncated to two equations and solved, yielding

$$F_x = \frac{32}{3} \left(1 - \frac{\beta + 2\gamma}{3} S + O(S^2) \right). \tag{4.15}$$

If S^2 is large, the evaluation of the integrals in (3.9) and (3.10) is obtained by following the procedure of Bleistein & Handelsman (1986). Starting from the Parseval formula

$$\int_0^\infty f(v)h(Sv) dv = \frac{1}{2\pi i} \int_{c-i\infty}^{c+i\infty} S^{-z} M[f; 1-z] M[h; z] dz, \tag{4.16}$$

where M denotes the Mellin transform, the large- S behaviour of (4.16) is obtained by pulling the contour of the right-hand integral to the right and computing the residues of the poles that are exposed. We have

$$\begin{aligned} M[h; z] &= \int_0^\infty J_{2m+1/2}(t) J_{2l+1/2}(t) t^{z-1} dt \\ &= \frac{2^{z-1} \Gamma(1-z) \Gamma\left(m+l + \frac{1+z}{2}\right)}{\Gamma\left(m-l+1 - \frac{z}{2}\right) \Gamma\left(l-m+1 - \frac{z}{2}\right) \Gamma\left(m+l + \frac{3-z}{2}\right)}, \end{aligned} \tag{4.17}$$

$$M[(t^2 - i)^{-1/2}; 1-z] = \frac{e^{i\pi z/4}}{2\sqrt{\pi}} \Gamma\left(\frac{1-z}{2}\right) \Gamma\left(\frac{z}{2}\right), \tag{4.18}$$

each of which has poles at $z = 1, 3, 5, \dots$. The consequent double pole at $z = 1$ in (4.16) yields

$$\begin{aligned} &\int_0^\infty \frac{1}{(v^2 - i)^{1/2}} J_{2m+1/2}(Sv) J_{2l+1/2}(Sv) dv \\ &\sim \frac{(-1)^{l+m}}{\pi S} e^{i\pi/4} \left[\ln S - \frac{i\pi}{4} - \gamma - \psi(m+l+1) - \psi\left(|m-l| + \frac{1}{2}\right) \right], \end{aligned} \tag{4.19}$$

where γ is Euler's constant and $\psi(x) = \Gamma'(x)/\Gamma(x)$. The residue at the double pole at $z = 1$ can be evaluated by taking limits from the strip of regularity. Thus,

$$\begin{aligned} &\int_0^\infty \frac{Sv}{\Lambda(Sv)} J_{2m+1/2}(Sv) J_{2l+1/2}(Sv) dv \\ &\sim \frac{(-1)^{l+m}}{\pi S} \left\{ 2e^{i\pi/4} \left[\ln(S/2) - \gamma - \psi(m+l+1) - \psi\left(|m-l| + \frac{1}{2}\right) \right] + q \right\} \end{aligned} \tag{4.20}$$

where q is given by the finite part integral

$$q = \text{f.p.} \int_0^\infty \frac{S}{\Lambda(Sv)} \frac{dv}{v} = \int_0^1 \left[\frac{S}{\Lambda(Sv)} - 2e^{i\pi/4} \right] \frac{dv}{v} + \int_1^\infty \frac{S}{\Lambda(Sv)} \frac{dv}{v}. \tag{4.21}$$

Thus, the matrix elements are $O(S^{-1} \ln S, S^{-1})$. Inverting the matrix cannot be carried out in a closed form without breaking up the $O(S^{-1})$ and $O(S^{-1} \ln S)$ terms, which is undesirable. However, because the right-hand side is $O(1)$, the resulting $\{b_m\}$ and $\{c_m\}$ must have orders that lie between S^{-1} and $(S \ln S)^{-1}$.

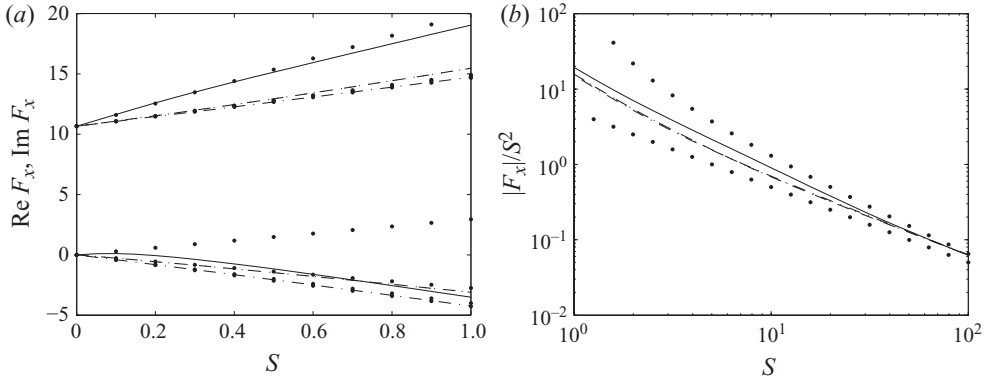


FIGURE 2. (a) Real and imaginary parts of F_x for $\omega/N = 0.1$ (solid curve), $1/2$ (dashed curve), 1 (dash-dotted curve) and 10 (dotted curve). The real parts tend to $32/3$ and the imaginary parts vanish at $S=0$. Dots indicate the asymptotic behaviour for small S . (b) $|F_x|/S^2$ for the same values of ω/N (same line styles), as well as the curves $5/S$ and $30/(S \ln S)$ (dots).

4.3. Numerical results

Numerical results of the infinite set of linear equations are obtained by calculating the matrix elements numerically using routine DQAGI of QUADPACK (Piessens *et al.* 1983) and truncating the sums at $m = M$. This leads to a square system of $2(M + 1)$ equations.

In general, the required values of M and N increase with increasing values of the disk radius (a) and with decreasing values of the viscosity parameter. For large a and small ν , the viscous effects are confined to a small boundary layer near the edge of the disk, and the modal summations (3.3) require several terms in order to resolve the velocity and pressure fields in this boundary layer. In practice, it was found that with $M = 2$, the relative change in the coefficients was less than 1% compared to the results with $M = 4$, so the results presented use $M = 2$. The coefficients show a clear exponential decay with m , indicating that the series is spectrally accurate.

Figure 2(a) shows the force coefficient $F_x = 2\sqrt{2\pi}(-2c_0 + b_0)$. For values of ω/N greater than $1/2$ or so, the curves are almost the same. The small- S behaviour is linear in S and is indicated in figure 2(a) by dots. For large ω/N , i.e. the elliptic case, this approximation is good for relatively large S . In the internal wave regime, the exact value of F_x rapidly departs from the asymptotic limit.

For large S , the non-dimensionalization used to define F_x is not helpful. The viscosity scales out of the more appropriate variable F_x/S^2 that is plotted in figure 2(b). The dashed and dot-dashed lines are proportional to S^{-1} and $(S \ln S)^{-1}$, respectively, these being the scaling bounds obtained previously.

The far-field pressure can be written as $p \propto \partial p_M / \partial x$, the x -derivative of a term that we call the equivalent monopole. The equivalent monopole is defined to be the non-dimensional quantity

$$p_M = - \int_0^\infty \frac{C(k)}{\sqrt{\frac{\omega^2}{4\nu^2} + \frac{iN^2k^2}{\omega\nu}}} \left[\frac{\lambda_1 e^{-\lambda_1|z|}}{\lambda_1^2 - k^2} - \frac{\lambda_2 e^{-\lambda_2|z|}}{\lambda_2^2 - k^2} \right] J_0(kr) dk. \quad (4.22)$$

Figure 3 shows the absolute value of this equivalent monopole multiplied by the distance from the origin $R \equiv a^{-1}\sqrt{r^2 + z^2}$. In the far field, $p_M R$ becomes a scattering cross-section independent of R from (4.5). The singularity of (4.5) is clearly visible on

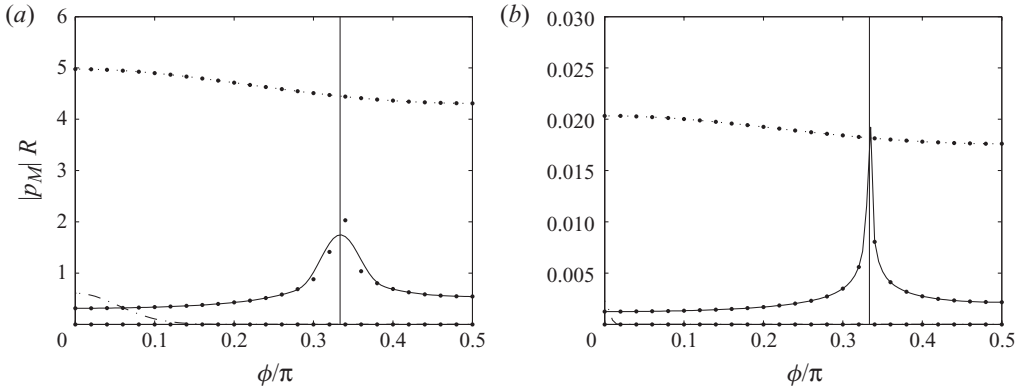


FIGURE 3. Equivalent monopole pressure cross-section $|p_M|R$ as a function of angle from the vertical, ϕ , for (a) $S = 1$, (b) $S = 100$ and $R = 100$. The solid curves correspond to $\omega/N = 1/2$, the dash-dotted curves to $\omega/N = 1$ and the dotted curves to $\omega/N = 2$. The dots and circles show the asymptotic solution (4.5), which is not valid for $\omega = N$. The vertical line corresponds to the angle of the St Andrews cross.

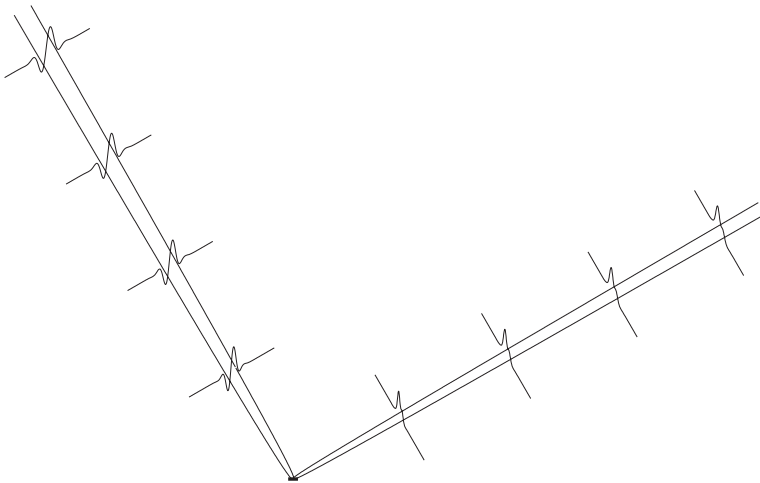


FIGURE 4. Energy flux along St Andrews cross and beam width $2(\beta z_+)^{1/3}$ for $S = 10$, (left half-plane) $\omega/N = \sqrt{3}/2$ and (right half-plane) $\omega/N = 1/2$. The scale for the energy flux is arbitrary. The disk (whose thickness is obviously not to scale) is visible at the origin of the beams.

the St Andrews cross. The curve for $\omega = N$ shows that the signal propagates in the vertical. As S increases, the scattering cross-section decreases in amplitude (in this normalization).

The energy flux per unit area is $\mathbf{I} = (\text{Re} [p\mathbf{v}^*])/2$. This is a vector quantity. Its component along the St Andrews cross is shown in figure 4 along with the beams emanating from the disk. It is natural to define coordinates along and perpendicular to the beam, z_+ and x_+ respectively, which are non-dimensional versions of the variable defined in Voisin (2003). The subscript $+$ is appropriate to the region above the disk, while x_+ points in the direction of energy propagation. The width of the beam scales like $|z|^{1/3}$ from (4.7). There is no difficulty defining a beam width because the disk provides a length scale.

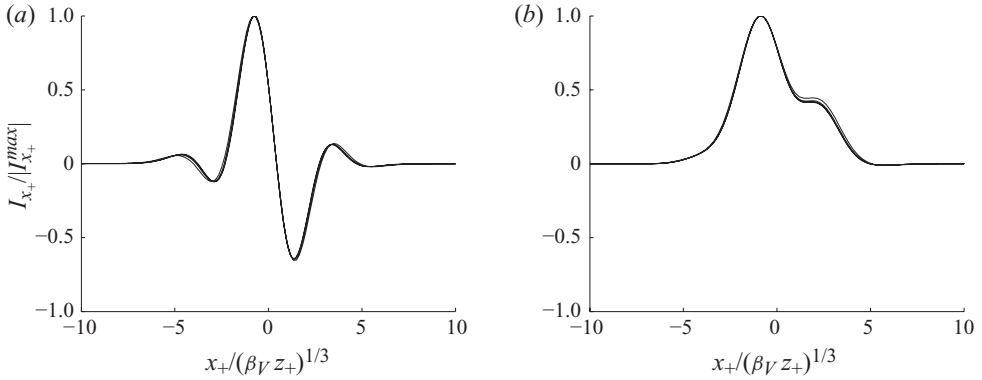


FIGURE 5. (a) Normalized energy flux for $S = 10$, (a) $\omega/N = \sqrt{3}/2$ and (b) $\omega/N = 1/2$ for $z_+ = 25, 50, 75, 100$.

Figure 5 shows the normalized energy flux along the St Andrews cross as a function of $x_+ / (\beta_V z_+)^{1/3}$. The factor $\beta_V \equiv \nu / 2N \sin \theta_0$ is included to make the plots directly comparable with those in Voisin (2003). The curves tend to functions of this variable and the curves for different distances from the origin are almost indistinguishable. The shape of the profile depends strongly on ω/N .

5. Comparison with the axisymmetric case

Viscosity is solely responsible for the generation of the wave field described above by edgewise oscillations of the disk. Such is not the case with broadside oscillations: then viscosity is expected to play a lesser role. Inviscid calculations were presented by Sarma & Krishna (1972), Lai & Lee (1981) and Gabov & Pletner (1988), while Bardakov, Vasil'ev & Chashechkin (2007) carried out viscous experiments.

The continuity equation (2.1) is satisfied by introducing the cylindrical velocity components $v_0 r^{-1}(-\partial\psi/\partial z, 0, \partial\psi/\partial r)$, in terms of which the only non-zero vorticity component is given by

$$\Omega_\theta = -\frac{v_0}{r} \left(\frac{\partial^2}{\partial r^2} - \frac{1}{r} \frac{\partial}{\partial r} + \frac{\partial^2}{\partial z^2} \right) \psi = -\frac{v_0}{r} L_{-1} \psi. \quad (5.1)$$

With the time dependence $e^{-i\omega t}$ already suppressed, substitution of (5.1) into (2.4) shows that the streamfunction satisfies

$$\frac{1}{r} \left(L_{-1} + \frac{i\omega}{\nu} \right) L_{-1} \psi = \frac{iN^2}{\omega\nu} \frac{\partial}{\partial r} \left(\frac{1}{r} \frac{\partial \psi}{\partial r} \right). \quad (5.2)$$

A suitable solution is

$$\psi(r, z) = \int_0^\infty F(k, z) r J_1(kr) dk, \quad (5.3)$$

where F satisfies (2.17). The condition $\partial\psi/\partial z = 0$ on the disk, $z = 0$, $r < a$, requires ψ to be an even function of z , vanishing at $z = 0$. Thus

$$\psi(r, z) = \int_0^\infty \left[\frac{e^{-\lambda_1|z|}}{\lambda_1} - \frac{e^{-\lambda_2|z|}}{\lambda_2} \right] \frac{A(k, z)}{k} r J_1(kr) dk, \quad (5.4)$$

which allows the pressure field to be deduced from (2.5) as

$$p = \frac{iN^2}{\omega} \rho_0 v_0 \operatorname{sgn}(z) \int_0^\infty \left[\frac{e^{-\lambda_1|z|}}{\lambda_1^2 - k^2} - \frac{e^{-\lambda_2|z|}}{\lambda_2^2 - k^2} \right] A(k, z) J_0(kr) dk. \tag{5.5}$$

So pressure discontinuities are confined to the disk provided

$$\int_0^\infty (\lambda_2^2 - \lambda_1^2) \frac{A(k)}{k^2} J_0(kr) dk = 0, \quad (r > a), \tag{5.6}$$

after use of (2.18). The prescribed broadside velocity of the disk is imposed by invoking (5.4) to obtain

$$\frac{1}{r} \left(\frac{\partial \psi}{\partial r} \right)_{z=0} = \int_0^\infty \left(\frac{1}{\lambda_1} - \frac{1}{\lambda_2} \right) A(k) J_0(kr) dk = 0, \quad (r < a). \tag{5.7}$$

The Tranter method is now applied, with $\alpha = 1/2$ as in § 3. Equation (5.6) is satisfied by writing

$$(\lambda_2^2 - \lambda_1^2) \frac{A(k)}{k^2} = (ka)^{1/2} \sum_{m=0}^\infty a_m J_{2m+1/2}(ka), \tag{5.8}$$

whose substitution in (5.7) gives

$$\sum_{m=0}^\infty a_m \int_0^\infty (ka)^{1/2} J_{2m+1/2}(ka) \frac{k^2 J_0(kr)}{\lambda_1 \lambda_2 (\lambda_1 + \lambda_2)} dk = 1, \quad (r < a). \tag{5.9}$$

Working as in § 3, the coefficients are shown to satisfy the linear system

$$\sum_{m=0}^\infty a_m \int_0^\infty \frac{v}{D(v)} \frac{J_{2m+1/2}(Sv) J_{2l+1/2}(Sv)}{[v^2 + i(N^2/\omega^2 - 1)]^{1/2}} dv = 2\delta_{l0} \sqrt{\frac{2}{\pi}}, \quad (l \geq 0). \tag{5.10}$$

The pressure jump at the disk yields a normal force $F = F_z \rho_0 v v_0 e^{-i\omega t} e_z$ with

$$F_z = -4\pi \int_0^a \int_0^\infty (\lambda_2^2 - \lambda_1^2) \frac{A(k)}{k} r J_0(kr) dk dr = -4\sqrt{2\pi} a_0 \tag{5.11}$$

after substitution of (5.8).

The small- S behaviour, obtained as in § 4, yields $F_z = -16(1 - \alpha S)$, with

$$\alpha = \frac{2}{\pi} \int_0^\infty \left[\frac{v^2}{D(v) [v^2 + i(N^2/\omega^2 - 1)]^{1/2}} - 1 \right] dv. \tag{5.12}$$

The $S=0$ value reproduces the known zero-frequency limit value for a broadside translating disk in creeping flow.

For large S , the results are non-uniform. When $\omega = N$, the integral in (5.10) reduces to the first integral in (3.9). As a result, the behaviour of the force is the same as in § 4. In particular, the force decays for large S . However, when $\omega \neq N$, the pole in (4.16) at $z = 1$ becomes a simple pole. The appropriate expansion is then

$$\int_0^\infty \frac{v}{D(v)} \frac{J_{2m+1/2}(Sv) J_{2l+1/2}(Sv)}{[v^2 + i(N^2/\omega^2 - 1)]^{1/2}} dv \sim \frac{(-1)^{l-m}}{\pi} M[f; 0] S^{-1} + \frac{2}{\sqrt{N^2/\omega^2 - 1}} M[h; 2] S^{-2} + O(S^{-3}). \tag{5.13}$$

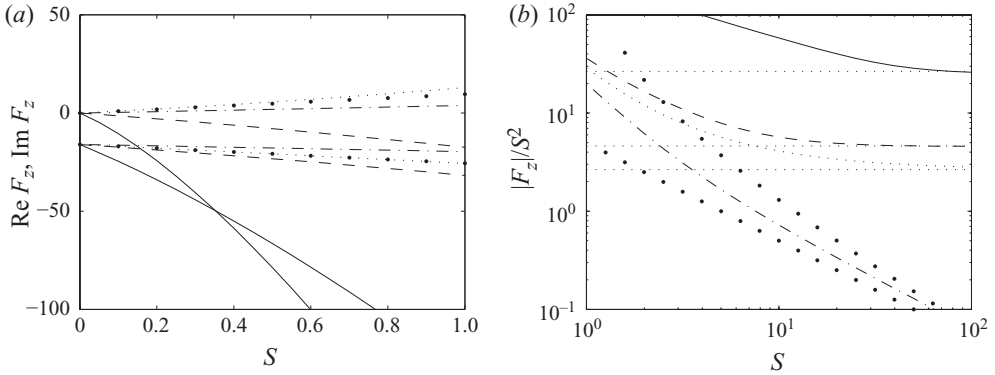


FIGURE 6. (a) Real and imaginary parts of F_z for $\omega/N = 0.1$ (solid curve), $1/2$ (dashed curve), 1 (dash-dotted curve) and 10 (dotted curve). The real parts tend to -16 and the imaginary parts vanish at $S=0$. Dots indicate the asymptotic behaviour for small S . (b) $|F_z|/S^2$ for the same values of ω/N (same line styles), as well as the curves $5/S$ and $30/(S \ln S)$ (dots) and the asymptotic values $(8/3)|N^2/\omega^2 - 1|^{1/2}$ (horizontal dotted curves).

Both terms are required to obtain the large- S behaviour of a_m . We find

$$M[h; 2] = (-1)^{l-m+1} |l-m| (l+m + \frac{1}{2}), \quad M[f; 0] = \int_0^\infty \frac{1}{D(v) \sqrt{v^2 + i(N^2/\omega^2 - 1)}} dv. \quad (5.14)$$

The matrix elements thus scale like $O(S^{-1})$. However, the leading-order matrix is singular, and in fact a_n are $O(S^2)$ and satisfy a homogeneous equation to leading order. One finds $a_0 = a_1 = (\sqrt{2/\pi}/3) S^2 \sqrt{N^2/\omega^2 - 1}$ and $a_n = O(S)$ for $N > 1$ in the limit of large S . The result for the force is $F_z = -(8/3) S^2 \sqrt{N^2/\omega^2 - 1}$. Hence, for large S , the force scaled appropriately for the inviscid limit, F_z/S^2 , tends to a constant, which is quite different from the edgewise case but not surprising. The dimensional result is $\mathbf{F} = -(8/3) \sqrt{N^2 - \omega^2} \rho_0 v_0 a^3 e^{-i\omega t} \mathbf{e}_z$, as in Lai & Lee (1981). Vertical oscillations remain an effective mechanism of excitation as the viscosity decreases while horizontal oscillations do not, because the latter impart motion to the fluid via the no-slip condition.

Figure 6 shows the non-dimensional force for $\omega/N = 0.1, 1/2, 1$ and 10 . The small- S asymptotic behaviour is poor for the $\omega = N$ case. For large S , the difference between the critical $\omega = N$ case, for which the scaled force decays as S increases, and the other three cases, for which it tends to a constant, is clear.

6. The effect of density diffusion

The results so far have concentrated on the effects of fluid viscosity, which affects the boundary condition on the surface of the disk as well as the nature of the wave field near the St Andrews cross. In a real fluid, density is not conserved along fluid particles and the energy equation becomes the advection–diffusion equation

$$\frac{\partial \rho}{\partial t} = \rho_0 \frac{N^2}{g} \mathbf{v} \cdot \mathbf{e}_z + \kappa \nabla^2 \rho. \quad (6.1)$$

The density diffusion coefficient κ appears and the Prandtl number $Pr \equiv \nu/\kappa$ (≈ 7 for water) becomes relevant. There have been some previous studies of internal

waves that explicitly considered diffusion, among others Thomas & Stevenson (1973), Kistovich & Chashechkin (1995) and Bardakov *et al.* (2007).

The analysis in §§ 2–5 can be carried out in an analogous fashion and only the main results are given here. The z -component of (2.7) is unchanged and hence the vertical vorticity is given by (2.8). Thus, density diffusion has no boundary layer analogous to the Stokes layer, which is due to the no-slip condition.

The counterpart of (2.17), which determines the internal wave dynamics, is

$$\left(\frac{d^2}{dz^2} - k^2\right) \left(\frac{d^2}{dz^2} - k^2 + \frac{i\omega}{\nu}\right) \left(\frac{d^2}{dz^2} - k^2 + \frac{i\omega}{\kappa}\right) F - \frac{N^2 k^2}{\nu\kappa} F = 0. \tag{6.2}$$

The auxiliary equation is now a bi-cubic rather than a bi-quadratic, and its solutions no longer take simple forms as in (2.18). They can be written $\pm\lambda_1, \pm\lambda_2, \pm\lambda_3$. Density diffusion adds another length scale to the problem, namely $\sqrt{\kappa/\omega}$.

The vertical velocity is then

$$V_z = \text{sgn}(z) \int_0^\infty \sum_{j=1}^3 C_j(k) e^{-\lambda_j|z|} \frac{J_1(kr)}{k} dk, \tag{6.3}$$

with $C_1 + C_2 + C_3 = 0$ ensuring that $V_z = 0$ on the plane $z = 0$. The density becomes, from (6.1),

$$\rho = -\frac{\rho_0 v_0 N^2}{g\kappa} \text{sgn}(z) \int_0^\infty \sum_{j=1}^3 \frac{C_j(k)}{\lambda_j^2 - k^2 + i\omega/\kappa} e^{-\lambda_j|z|} \frac{J_1(kr)}{k} dk. \tag{6.4}$$

The appropriate boundary condition is no flux of density through the disk, but symmetry considerations show that this holds over the entire plane $z = 0$. Hence

$$\sum_{j=1}^3 \frac{\lambda_j C_j(k)}{\lambda_j^2 - k^2 + i\omega/\kappa} = 0. \tag{6.5}$$

The same procedure as previously gives the zonal velocity components, from which it is found that the pair of velocity conditions (2.26) and (2.27) has $k^{-2} \sum_{j=1}^3 \lambda_j C_j(k)$ instead of $aC(k)/\Lambda(ka)$ and the pair of stress conditions (2.29) and (2.30) has $k^{-2} \sum_{j=1}^3 \lambda_j^2 C_j(k)$ instead of $2C(k)$. The application of Tranter’s method proceeds as above and the resulting dual integral equations (3.6) and (3.7) have $a/\Lambda(u)$ replaced by

$$2 \frac{\sum_{j=1}^3 \lambda_j C_j(k)}{\sum_{j=1}^3 \lambda_j^2 C_j(k)} = 2 \frac{\begin{vmatrix} \lambda_1 & \lambda_2 & \lambda_3 \\ 1 & 1 & 1 \\ \lambda_1 & \lambda_2 & \lambda_3 \end{vmatrix}}{\begin{vmatrix} \lambda_1^2 - k^2 + i\omega/\kappa & \lambda_2^2 - k^2 + i\omega/\kappa & \lambda_3^2 - k^2 + i\omega/\kappa \\ \lambda_1^2 & \lambda_2^2 & \lambda_3^2 \\ 1 & 1 & 1 \\ \lambda_1 & \lambda_2 & \lambda_3 \end{vmatrix}}. \tag{6.6}$$

This ratio of determinants clearly exhibits the algebraic effect of introducing density diffusion. However, the counterpart of (3.8) is the trio of roots of

$$\left[\left(\frac{\lambda a}{S}\right)^2 - v^2\right] \left[\left(\frac{\lambda a}{S}\right)^2 - v^2 + i\right] \left[\left(\frac{\lambda a}{S}\right)^2 - v^2 + iPr\right] = \frac{N^2}{\omega^2} Pr v^2, \tag{6.7}$$

deduced from (6.2).

At small k , the $O(k^3)$ term in λ_1 has $(\nu + \kappa)$ instead of ν in (4.6) and this change, equivalent to the factor $(1 + Pr^{-1}) \approx 8/7$ for water, appears in the far-field pressure estimate (4.7). The asymptotic behaviour outside the cone is unchanged, but the beams are broadened by a factor of $(1 + Pr^{-1})^{1/3}$, which is a very small correction for water (2.3 %). At large k ,

$$\lambda_j^2 - k^2 = \mu_j, \quad (\mu_1, \mu_2, \mu_3) \sim (e^{i\pi/3}, -1, e^{-i\pi/3}) \left(\frac{N^2 k^2}{\nu \kappa} \right)^{1/3}, \quad (6.8)$$

and the ratio of determinants is asymptotically k^{-1} again.

The asymptotic analysis of §4 carries through to the present section. The scalings remain unchanged, as does β of (4.13), but the coefficients γ and q of (4.14) and (4.21) now incorporate a dependence on Prandtl number that involves the above cubic roots. The numerics are more complicated but basically the same and therefore omitted. Hence, as found in previous studies, density diffusion has a very minor effect. Naturally, density diffusion can also be incorporated in the axisymmetric problem.

7. Summary

A complete solution is derived for the wave field due to an edgewise oscillating horizontal circular disk in an incompressible stratified viscous fluid. The viscous decay length assumes a fundamental role and the Stokes number takes account of the disk radius. Large values of S^2 produce the familiar inviscid beams but small values reveal how viscosity can modify the ‘St Andrew’s cross’ beams. Broadside oscillations, included for comparison, remain an effective excitation mechanism as the viscosity is reduced, because they do not rely on the no-slip condition. The addition of density diffusion complicates the mathematics but barely affects the physical features.

We thank an anonymous reviewer for a very careful reading of the manuscript and detailed comments.

REFERENCES

- ABRAMOWITZ, M. & STEGUN, I. A. 1965 *Handbook of Mathematical Functions*. Dover.
- BARDAKOV, R. N., VASIL'EV, A. Y. & CHASHECHKIN, Y. D. 2007 Calculation and measurement of conical beams of three-dimensional periodic internal waves excited by a vertically oscillating piston. *Fluid Dyn.* **42**, 612–626.
- BLEISTEIN, N. & HANDELSMAN, R. A. 1986 *Asymptotic Expansions of Integrals*. Dover.
- DAVIS, A. M. J. 1993 Some asymmetric Stokes flows that are structurally similar. *Phys. Fluids A* **5**, 2086–2094.
- DAVIS, A. M. J. & NAGEM, R. J. 2004 Effect of viscosity on acoustic diffraction by a circular disk. *J. Acoust. Soc. Am.* **115**, 2738–2748.
- ERMANYUK, E. V. & GAVRILOV, N. V. 2008 On internal waves generated by large-amplitude circular and rectilinear oscillations of a circular cylinder in a uniformly stratified fluid. *J. Fluid Mech.* **613**, 329–356.
- GABOV, S. A. & PLETNER, Y. D. 1988 The problem of the oscillations of a flat disk in a stratified liquid. *Comput. Math. Math. Phys.* **28**, 41–47.
- GARRETT, C. & KUNZE, E. 2007 Internal tide generation in the deep ocean. *Annu. Rev. Fluid Mech.* **39**, 57–87.
- GORDON, D. & STEVENSON, T. N. 1972 Viscous effects in a vertically propagating internal wave. *J. Fluid Mech.* **56**, 629–639.
- GÖRTLER, H. 1943 Über eine Schwingungerscheinung in Flüssigkeiten mit stabiler Dichteschichtung. *Z. Angew. Math. Mech.* **23**, 65–71.

- HURLEY, D. G. & HOOD, M. J. 1997 The generation of internal waves by vibrating elliptic cylinders. Part 3. Angular oscillations and comparison of theory with recent experimental observations. *J. Fluid Mech.* **433**, 61–75.
- HURLEY, D. G. & KEADY, G. 1997 The generation of internal waves by vibrating elliptic cylinders. Part 2. Approximate viscous solution. *J. Fluid Mech.* **351**, 119–138.
- KISTOVICH, Y. & CHASHECHKIN, Y. D. 1995 The reflection of beams of internal gravity waves at a flat rigid surface. *J. Appl. Maths Mech.* **59**, 579–585.
- KISTOVICH, Y. V. & CHASHECHKIN, Y. D. 2001 Some exactly solvable problems of the radiation of three-dimensional periodic internal waves. *J. Appl. Mech. Tech. Phys.* **42**, 228–236.
- LAI, R. Y. S. & LEE, C.-M. 1981 Added mass of a spheroid oscillating in a linearly stratified fluid. *Intl J. Engng Sci.* **19**, 1411–1420.
- LIGHTHILL, M. J. 1978 *Waves in Fluids*. Cambridge University Press.
- MOWBRAY, D. E. & RARITY, B. S. H. 1967 A theoretical and experimental investigation of the phase configuration of internal waves of small amplitude in a density stratified liquid. *J. Fluid Mech.* **28**, 1–16.
- MUNK, W. & WUNSCH, C. 1998 Abyssal recipes. II. Energetics of tidal and wind mixing. *Deep Sea Res.* I **45**, 1977–2010.
- PIESSENS, R., DE DONCKER-KAPENGA, E., ÜBERHUBER, C. W. & KAHANER, D. 1983 *Quadpack: A Subroutine Package for Automatic Integration*. Springer.
- RAYLEIGH, LORD 1883 Investigation of the character of the equilibrium of an incompressible heavy fluid. *Proc. Lond. Math. Soc.* **9**, 57–70 (also in *Scientific Papers*, **2**, 200–207, Cambridge University Press, 1900).
- SARMA, L. V. K. & KRISHNA, D. V. 1972 Oscillation of axisymmetric bodies in a stratified fluid. *Zastosow. Matem.* **13**, 109–121.
- SNEDDON, I. N. 1966 *Mixed Boundary Problems in Potential Theory*. North-Holland.
- SUTHERLAND, B. R. & LINDEN, P. F. 2002 Internal wave excitation by a vertically oscillating elliptical cylinder. *Phys. Fluids* **14**, 721–731.
- TANZOSH, J. P. & STONE, H. A. 1995 Transverse motion of a disk through a rotating fluid. *J. Fluid Mech.* **301**, 295–324.
- THOMAS, D. N. & STEVENSON, T. N. 1972 A similarity solution for viscous internal waves. *J. Fluid Mech.* **54**, 495–506.
- THOMAS, N. H. & STEVENSON, T. N. 1973 An internal wave in a viscous ocean stratified by both salt and heat. *J. Fluid Mech.* **61**, 301–304.
- TRANTER, C. J. 1966 *Integral Transforms in Mathematical Physics*. Wiley.
- VASIL'EV, A. Y. & CHASHECHKIN, Y. D. 2006 Generation of beams of three-dimensional periodic internal waves by sources of various types. *J. Appl. Mech. Tech. Phys.* **47**, 314–323.
- VOISIN, B. 2003 Limit states of internal wave beams. *J. Fluid Mech.* **496**, 243–293.